# Nanoscale dissipation and magnetoresistive $1/f$ noise in spin valves

Zhu Diao,[1] E. R. Nowak,[1,2] K. M. Haughey,[2,*] and J. M. D. Coey[1]

[1]*School of Physics and CRANN, Trinity College, Dublin 2, Ireland*
[2]*Department of Physics and Astronomy, University of Delaware, Newark, DE 19716, USA*

Spatial correlations of $1/f$ noise in yoke-shaped, giant magnetoresistance spin valve sensors are reported. An upper bound of 135 nm, corresponding to a magnetic volume of $<10^5$ nm$^3$, is determined for the lateral size of the magnetic fluctuators responsible for the magnetoresistive $1/f$ noise in regions where the resistance susceptibility is large. The normalized noise power is found to scale inversely with the separation between voltage taps along the arm of the yoke, also consistent with a local noise mechanism. The magnetoresistive $1/f$ noise is associated with quasiequilibrium fluctuations in the micromagnetic structure having a length scale set by the disorder formed during the deposition and processing of the materials stack.

## I. INTRODUCTION

Studies of magnetic noise date back to early work by Barkhausen[1] on domain wall motion in ferromagnets. In many systems, such as soft amorphous magnets,[2] spin glasses,[2,3] and even nominally nonmagnetic surfaces and interfaces,[4] the spectral density of the magnetic fluctuations exhibits an increase with decreasing frequency $f$ that is approximately proportional to $1/f$. The measured spectral density of the magnetic noise and the dissipative part of the magnetic susceptibility are often found to satisfy the fluctuation–dissipation relationship.[2,5] Although this indicates that the magnetic $1/f$ noise is a thermal and equilibrium one, the underlying mechanisms of the magnetic fluctuations are less clear. They usually involve, e.g., transitions of domain walls over energy barriers, tunneling of magnetization, or hopping of various structural defects, and invoke a distribution of metastable states created by disorder that leads to the formation of a $1/f$ noise spectrum. Recently, surface spin relaxation phenomena have been implicated as a source of $1/f$ magnetic flux noise in superconductors, which had been a puzzle for nearly 30 years.[6]

Magnetic $1/f$ noise can also be a dominant source of interference in spin-based magnetoelectric devices,[7] which consist of layered structures of magnetic and nonmagnetic thin films. One such device is the spin valve (SV). It consists of two ferromagnets that are separated by a thin normal metal spacer. The interplay between magnetism and electric currents in such structures leads to giant magnetoresistance (GMR) and tunneling magnetoresistance (TMR). However, a comprehensive understanding of coupled current and magnetization noise in magnetoelectric structures is lacking and is of recent theoretical interest, particularly in nanostructures.[8] SVs provide a means to indirectly measure the magnetization noise in such structures via resistance fluctuations.

Further investigations of magnetic noise and related energy dissipation are of great practical importance for miniaturizing and improving the performance of spin-based electronic devices, such as magnetic random access memory[9] and magnetic field sensors,[10] and for guiding the search for low loss materials in superconducting qubit circuits used for quantum information processing.[11]

GMR and TMR magnetic field sensors are known to exhibit excess low-frequency resistance noise with a $1/f$ power spectrum.[10,12,13] In general, the power spectral density of the resistance fluctuations is well described by a Hooge-like expression[14]

$$S_R(f) = \alpha \frac{R^2}{\Omega f^\beta},$$

where $R$ is the direct current (DC) resistance, $f$ is the frequency, $\beta$ is the spectral slope, and $\Omega$ is the volume.

The Hooge parameter $\alpha$ may have contributions from both electronic and magnetic mechanisms.[15] Thermal magnetization fluctuations, in particular, lead to magnetoresistive (MR) noise that limits the sensitivity of GMR and TMR sensors at low frequencies.[12,16–18] Equilibrium magnetization noise is related to the out-of-phase magnetic susceptibility $\chi_M''(f)$ through the fluctuation dissipation theorem,[12] i.e.,

$$S_M(f) = \chi_M''(f)(2k_B T/\pi \Omega \mu_0 f).$$

MR noise that has a $1/f$ spectrum therefore requires that the dissipative component of the magnetic susceptibility be independent of frequency at low frequencies. For single magnetic domain particles, the solution to the Landau-Lifshitz-Gilbert equation yields $\chi_M'' \sim f$ in the low-frequency limit, roughly $<1$ GHz. This results in magnetic white noise that has a frequency-independent power spectrum, rather than a $1/f$ spectrum.[19] The nature of the fundamental fluctuating magnetic entities that give rise to stationary MR $1/f$ noise in SVs is still emerging; it has been associated with metastable magnetic microstructure in the magnetic layers of the SV[12,15,20] and with a Jordan-type magnetic aftereffect.[17]

In ferromagnetic materials and heterostructures, a number of magnetic length scales exist as a result of the interplay among magnetostatic, anisotropy, and exchange energies. In this regard, spatial correlations of the MR $1/f$ noise are of fundamental interest for revealing the length scales over which dissipation occurs in nanometer-thick magnetic films. Experimental studies of the spatial correlations of magnetic noise are sparse. For example, Raquet *et al.*[21] reported no spatial correlation of the fluctuations between two adjacent Hall bars patterned from a thin film of nickel and concluded that the magnetic $1/f$ noise was uncorrelated on the scale of

600 nm. However, investigations of the correlation length scale for MR $1/f$ noise in materials stacks used for SV magnetic sensors are lacking yet remain important for guiding the development of theoretical models for the magnetic noise in magnetoelectric heterostructures, micromagnetic simulations, and materials improvement and processing. In addition to magnetoelectric devices, studies of the spatial correlation of magnetic noise maybe of potential importance for improving superconducting quantum interference device magnetometry and qubits by further revealing the role of interactions and collective effects between surface spins in generating $1/f$ flux noise.[11]

Here, we report on the spatial correlations of the MR $1/f$ noise in GMR SVs. Fluctuations between adjacent voltage taps are mainly uncorrelated, particularly for the exchange-pinned layer, and indicate that the lateral length scale for spatial correlations is less than the minimum separation between voltage taps, i.e., 300 nm. Moreover, the normalized noise is found to scale inversely with the distance between voltage taps. The data indicate that the mechanism for MR $1/f$ noise is local and results from a distribution of magnetic fluctuators, which are defined by the disorder formed during the deposition of the magnetic layers.

## II. EXPERIMENTAL METHODS

Sputter-deposited SVs were patterned into yoke-shaped devices that have the crossed-anisotropy configuration used for a magnetic field sensor. The yoke-shaped design (Fig. 1) promotes a stable domain structure in the long arm of the yoke, reducing "burst" noise associated with macroscopic domain wall motion.[22] Yoke SV sensors were originally designed for tape heads, and they have been used more recently by Pannetier *et al.* in a mixed sensor.[23] The yoke is patterned relative to the exchange-bias direction, which was set by the application of a 20-mT magnetic field during film deposition. The crossed anisotropy required for a linear response is illustrated in Fig. 2(a). It is established by having the top magnetic layer exchange-bias pinned in a direction perpendicular to the long arm of the yoke, while shape anisotropy ensures that the bottom (so-called free) magnetic layer's easy-axis is along the arm. The field to be sensed is then applied in plane and transverse to the long arm, as depicted in the top panel in Fig. 2. Ideally, this causes the free layer to rotate coherently, which yields a linear, low hysteresis transfer curve in the MR response around a zero field suitable for sensor applications. Another commonly used configuration is illustrated in Fig. 2(b). It involves collinear anisotropy, wherein the shape anisotropy direction of the free layer and the exchange-bias direction of the reference layer are set to lie along the same axis. This causes the magnetizations in the two layers to be aligned either parallel or antiparallel to one another in a zero-applied field.

Three types of SV devices were produced from stacks deposited using a Shamrock sputtering tool: the SV stack used in type A devices was Si/SiO$_2$/Ta (5)/NiFe (3.5)/CoFe (5)/Cu (2.4)/CoFe (3.5)/IrMn (10)/Ta (5), and for both B and C devices, it was Si/SiO$_2$/Ta (5)/NiFe (3.5)/CoFe (1.5)/Cu (2.9)/CoFe (2.5)/IrMn (10)/Ta (5), where the parenthetical numbers indicate the layer thickness in nanometers. Similar materials stacks are used to fabricate commercially available GMR magnetic sensors for low-frequency applications. Stacks were patterned using photolithography and electron beam lithography followed by argon ion milling. The dimensions of the yoke structures are denoted in micrometers as $(w, l, m)$, where $w$ is the width of the yoke arm, $l$ is the length of the whole yoke structure, and $m$ is the transverse dimension of the yoke
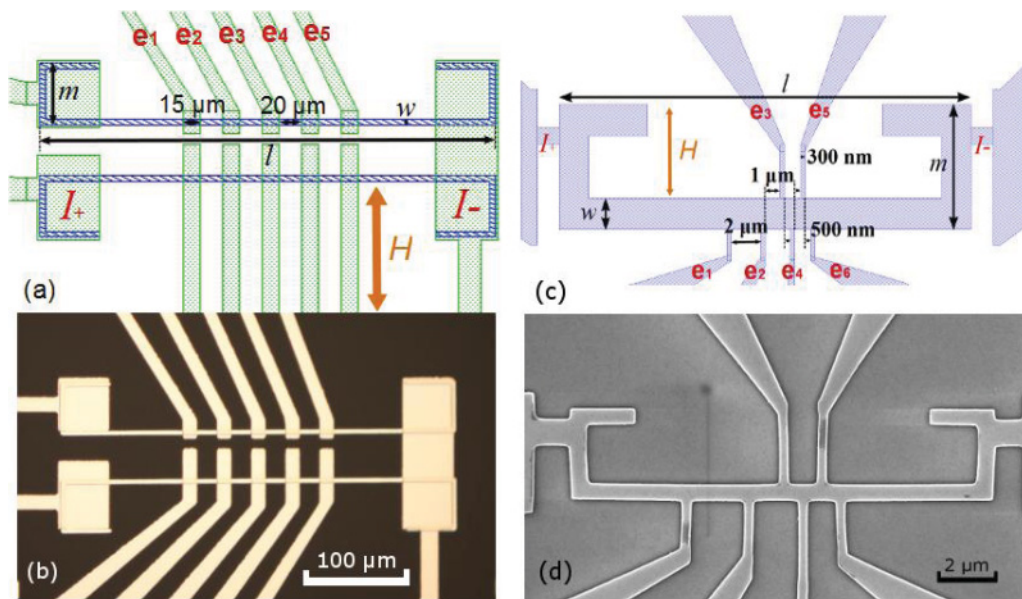


FIG. 1. (Color online) (a) The pattern design for type A yoke devices. (b) An optical image of a type A device that has equally spaced voltage taps. (c) The pattern design used for type B and C devices. (d) A scanning electron microscopy image of a type C yoke SV structure with a 600-nm width patterned by single-step electron beam lithography. An external magnetic field is applied perpendicular to the long arm of the yoke structure, and a bias current is injected at the ends of the yoke's long arm. The corresponding dimensions and labels for electrodes in (a) and (c) are listed in Table I.
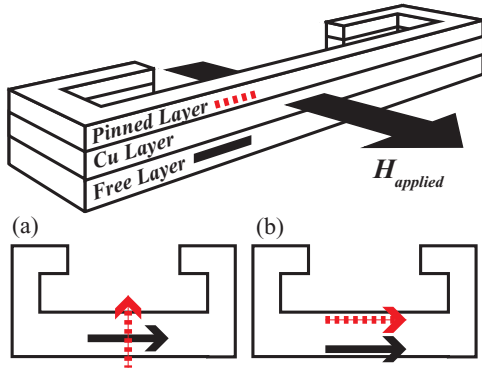
FIG. 2. (Color online) Sketches illustrating the yoke geometry and devices that have (a) crossed-anisotropy and (b) collinear anisotropy configurations for the pinned and free magnetic layers. The arrows in (a) and (b) depict the nominal orientation of the magnetization in the two layers in the zero-applied field for crossed and collinear anisotropy, respectively. For both cases, the external field was applied perpendicular to the long arm of the yoke, as indicated in the top panel.

(see Figs. 1(a) and 1(c) and Table I). The dimensions were (5.0, 405, 55) for type A, (2.0, 16.0, 6.0) for type B, and (0.6, 15.6, 3.6) for type C. Electric contacts to type A yokes were made by depositing copper electrodes directly on top of the yoke [as shown in Fig. 1(b)] in a second lithography step followed by liftoff. Contacts to type B and C devices were patterned directly into the multilayer stack [see the scanning electron microscopy image in Fig. 1(d)]. Although the micromagnetics of the yoke arm are altered slightly in the latter case, these contacts had much lower resistance and added no excess noise. Voltage contacts in type A samples were designed with a uniform 20-$\mu$m spacing; the spacing between adjacent voltage contacts (labeled $e_1$ to $e_6$) for type B and C devices is listed in Table I.

## III. RESULTS

Conventional four-probe MR and voltage noise measurements were performed under constant current bias.[16] A current of 250 $\mu$A was typically applied. The magnetic field dependence was measured by varying the applied field $\mu_0 H$ incrementally, typically in steps of 0.5 mT, from positive saturation to negative saturation and back. The 0.5-mT changes in field were made by ramping the current in the electromagnet linearly in time at a rate of 0.1 mT/s. The applied magnetic

TABLE I. Dimensions (in micrometers) of the yoke devices and spacing between adjacent electrodes. $w$ denotes the width of the yoke arm, $l$ is the length of the entire yoke structure, and $m$ is the transverse dimension of the yoke. Columns labeled $e_{XY}$, where $X$ and $Y$ are numbers, list the spacing between adjacent voltage contacts [see also Figs. 1(a) and 1(c)]. The nominal yoke resistance between $e_{12}$ was 65, 23, and 67 $\Omega$ for type A, B, and C samples, respectively.

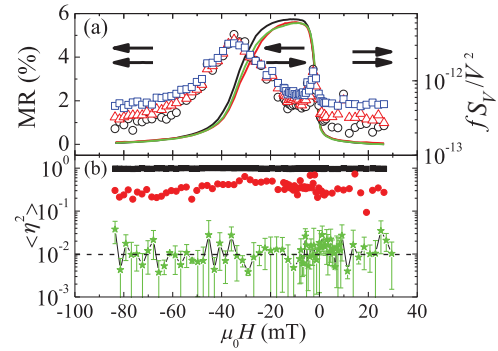| Sample set | $w$ | $l$ | $m$ | $e_{12}$ | $e_{23}$ | $e_{34}$ | $e_{45}$ | $e_{56}$ |
|---|---|---|---|---|---|---|---|---|
| A | 5.0 | 405 | 55 | 20 | 20 | 20 | 20 | |
| B | 2.0 | 16.0 | 6.0 | 2.0 | 1.0 | 0.5 | 0.5 | 0.5 |
| C | 0.6 | 15.6 | 3.6 | 2.0 | 1.0 | 0.5 | 0.5 | 0.5 |



FIG. 3. (Color online) Plotted in (a) are the MR and normalized noise as a function of magnetic field for a $w = 5$ $\mu$m yoke type A device. Data were taken at a 250-$\mu$A DC bias, and the MR curves (black, red, and green) were measured for different pairs of voltage taps. Noise peaks at $-40$ and 0 mT correspond to the switching of the pinned and free magnetic layers, respectively. The noise data at 5, 10, and 20 Hz are indicated by circles (black), triangles (red), and squares (blue), respectively. (b) Ensemble-averaged coherence function $\eta_{12}^2$ between 4 and 8 Hz for different electrodes pairs: ■ ($e_{45}$) (black), ● ($e_{35}$ and $e_{34}$) (red), and ★ ($e_{34}$ and $e_{45}$) (green). The dashed line is a guide to the eye.

field was held constant during the course of the measurements of the resistance and the averaged noise spectrum. Typically, measurements at each field took $\sim$60 s and were started 60 s after the field set point was reached. For relaxation studies, discussed later, both the measurement duration and the delay time were reduced to measure the resistance and noise at shorter times (down to a few seconds), but at the expense of less averaging. Solid lines in Fig. 3(a) show representative MR curves for different voltage contact pairs in a type A device. The curves are practically equivalent in terms of MR and switching fields. The power spectral density of the voltage fluctuations $S_V$ was measured between 1 and 1000 Hz, corrected for background noise from the electronic instrumentation, and then normalized by $f/V,^2$ where $V$ is the DC voltage across the respective contact pair. The normalized noise $f S_V / V^2$ is also plotted in Fig. 3(a) using symbols for three frequencies: 5, 10, and 20 Hz. When the device is at positive saturation, only thermal (Johnson) background noise is measured. There is a peak of the noise power near 0 mT during the magnetic reversal of the free layer. The noise then decreases when the two ferromagnetic layers are in an antiparallel configuration. Another pronounced peak in noise power occurs during the reversal of the pinned layer. Finally, the noise drops to the same thermal background level when negative saturation fields are reached. The quantity $f S_V / V^2$ will be a constant at all frequencies for $1/f$ noise, and it will increase linearly with $f$ for the background thermal (white) noise. The data in Fig. 3(a) indicate that during the magnetization reversal, the low-frequency magnetic noise has a $1/f$ spectrum. Spectrum 3 in Fig. 4 is an example of a $1/f$ spectrum measured near the peak in noise power due to the reversal of the pinned layer in a type A device.

The noise in the reversal regions is attributed to equilibrium magnetization fluctuations[16] or irreversible magnetization creep,[24] which couple to the resistance through the GMR effect. Over a period from $10^1$ to $10^5$ s after a 0.5-mT step
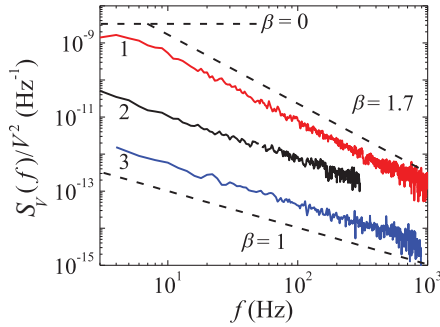
FIG. 4. (Color online) Voltage noise power spectral densities measured in a type A device and a type B device that has collinear anisotropy. Spectrum 3 for the type A device was measured near $-35$ mT in Fig. 3, corresponding to the reversal of the pinned layer. The spectrum is very close to $1/f$. For the type B device, a Lorentzian-like spectrum (spectrum 1) is observed across $e_{46}$ at 9 mT, where the coherence for $e_{23}e_{46}$ is largest (see Fig. 8). In contrast, a $1/f$-like spectrum (spectrum 2) is found at $-12$ mT, where the coherence is small and close to 0.01.

change in the applied field is made, the resistance relaxation due to the free layer is small; e.g., in the type A sensor device, it is $\sim$0.6%. Furthermore, most of the change in MR $1/f$ noise power (up to a factor of 2) occurs in the first 100 s (1000 s for the pinned layer) after the applied field is changed; at longer times, the magnitude is stationary and the frequency dependence is still very close to $1/f$. Hence, the $1/f$ spectra we observe from 1 to $10^3$ Hz are associated with dissipative, relaxation processes resulting from perturbations due to thermal fluctuation fields $\delta\mu_0 H \propto S_R^{1/2}(dR/d\mu_0 H)^{-1}$, which are of the order 0.1 $\mu$T in our devices.

For stationary, equilibrium magnetic $1/f$ noise, $\alpha$ often exhibits a linear dependence on the normalized resistance susceptibility, $1/R(dR/d\mu_0 H)$.[16,25] This linear dependence is evident in the compilation plot shown in Fig. 5 and confirms that the noise near the switching fields is equilibrium noise of magnetic origin for all of our devices. Moreover, the Hooge-like parameters for different electrode pairs on the same device coincide, indicating that $\alpha$ is independent of the volume of sample being probed; i.e., the fluctuating entities are small in
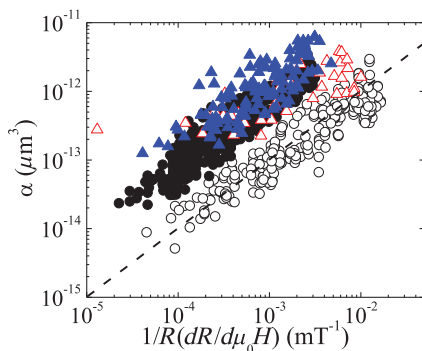


FIG. 5. (Color online) Hooge parameter during magnetization switching plotted against $1/R(dR/d\mu_0 H)$ for different volume sections in type A (circles) and B (triangles) samples. Free and pinned layers are depicted by open and solid symbols, respectively. The dashed line has unit slope and is a guide to the eye.
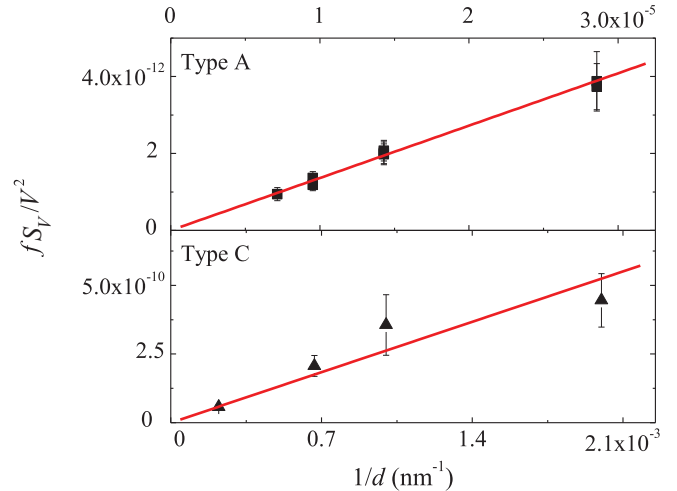


FIG. 6. (Color online) Normalized noise power plotted as a function of the inverse of the voltage tap separation $d$ in a type A (squares) and a type C (triangles) device. Data are shown for noise measured in the region of the pinned and free magnetic layer's reversal for the type A and C device, respectively. Solid lines are linear fits to the data forced through the origin.

comparison to the sample volume. This is further corroborated by Fig. 6, which shows that the normalized noise powers in a type A and a type C device scale inversely with voltage tap separation.

Spatial correlations of the MR noise between pairs of voltage electrodes were quantified by computing an ensemble-averaged coherence function defined as

$$\eta_{12}^2(f) = \frac{|S_{12}(f)|^2}{S_1(f)S_2(f)},$$

where $S_{12}$ is the cross-power spectral density of the two signals and $S_1$ and $S_2$ are the individual voltage spectra measured across different voltage taps. The statistical error for the average coherence scales as $1/N$, where $N$ is the number of averages; $N = 100$ for our data.

In Fig. 3(b), we plot $\eta_{12}^2$ as a function of field for different electrode pairs in a $w = 5$ $\mu$m (type A) yoke. For a single pair of electrodes, $e_{45}$, $\eta_{12}^2 = \eta_{11}^2 \approx 1$ as expected. $\eta_{12}^2(f)$ decreases whenever the sample's MR $1/f$ noise becomes comparable to the background noise, which is mostly incoherent noise from the amplifiers. The decrease is usually observed at high frequencies and near saturation, where the MR $1/f$ noise is greatly reduced. This effect can be corrected using the procedure detailed in Ref. 26. After correction, $\eta_{12}^2(f)$ was found to be independent of frequency out to at least 1 kHz at all fields. We report the mean value of the coherence function for frequencies $<$50 Hz to avoid artifacts associated with power line pickup. For adjacent electrode pairs (e.g., $e_{34}$ and $e_{45}$), $\eta_{12}^2 \approx 0.01$ near the reversal fields, indicating negligible spatial correlation. Finally, $\eta_{12}^2 \approx 0.25$ when half the volume is shared between electrodes, such as between $e_{35}$ and $e_{34}$. The ensemble-averaged coherence function can miss correlations that are phase shifted along the length of the yoke arm. However, there was no evidence of this in the imaginary part of the cross spectrum, which was featureless. These results indicate that the lateral length scale of the fluctuating magnetic
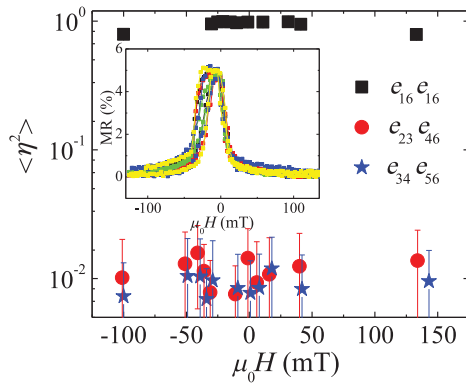
FIG. 7. (Color online) Ensemble-averaged coherence function between 18 and 42 Hz for a type C device and its MR curves (inset) measured across corresponding electrode pairs.

entities is necessarily $<20\,\mu$m, the separation between any pair of adjacent electrodes.

Figure 7 shows the corresponding results for a $w = 0.6\,\mu$m (type C) yoke sample that has a variable spacing of 0.5–2.0 $\mu$m between adjacent electrodes. The MR curves from different sections along the yoke are less uniform than for the $w = 5\,\mu$m yoke device, suggesting nonuniform magnetization of the magnetic layers in the active volume of the sample. The averaged coherence function shows similar behavior compared to that observed in larger-scale yokes. When the same electrode pair is measured, $\eta_{12}^2 \approx 1$ was observed. At saturation in high fields, $\eta_{12}^2$ is reduced to 0.8 due to incoherent background noise. Near the magnetization reversal fields, $\eta_{12}^2 \approx 0.01$ was observed again for adjacent electrode pairs, which is 0 within the statistical error. Hence, we conclude that the spatial correlation length of MR $1/f$ noise is less than a few hundred nanometers.

Figure 8 shows the averaged coherence and a representative MR curve ($e_{12}$) for a $w = 2\,\mu$m (type B) yoke device, in which the yoke arm was patterned to be along the exchange-bias pinning direction. This device has collinear anisotropy, rather than crossed anisotropy. Although not suitable as a sensor, the magnetization reversal in this device shows the influence
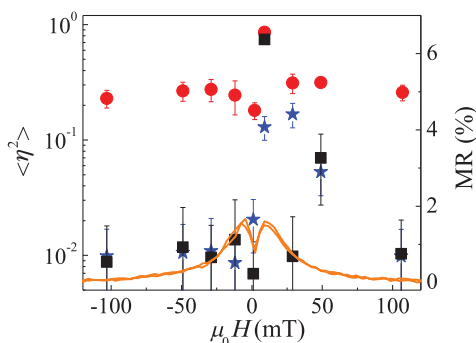


FIG. 8. (Color online) The MR curve measured for $e_{12}$ on a type B device, with the easy-axis of the free layer and the pinned layer both along the long arm of the yoke. Symbols represent the ensemble-averaged coherence function between 18 and 42 Hz as a function of applied magnetic field measured for $e_{23}e_{46}$ (■, black), $e_{46}e_{45}$ (●, red), and $e_{34}e_{56}$ (★, blue).

of macroscopic domain wall motion on the noise and spatial coherence. Under the zero-applied field, the free layer and the pinned layer are practically aligned in the same direction; a small angle between their respective magnetization may be caused by misalignment during the patterning process. When a magnetic field is applied transverse to the yoke arm, both the free and the pinned layers align along the field direction, with the free layer leading. Hence, the MR first increases as the angle between the two layers increases. After the free layer magnetization is aligned with the applied field, further increase in field aligns the pinned layer, reducing the angle and causing the resistance to decrease and then saturate when the magnetizations of the two layers are parallel.

At positive and negative saturation in Fig. 8, the coherence for all three electrode pairs investigated is as expected for a system without spatial correlation. Because the volume of electrode pair $e_{46}$ is twice that of $e_{45}$, we expect $\eta_{12}^2 \approx 0.25$ in the absence of spatial correlations, which is close to what is measured. However, during magnetization reversal, there is an increase in the coherence function for all three electrode pairs. The value of the coherence function varied depending on the electrode pairs, but it did not show a distinct trend. Noise spectra were measured at 9 mT, where the coherence is largest. At this field, most of the resistance change is due to the free layer. The spectra exhibited strong deviations from a $1/f$ slope that were characteristic of Lorentzian-like spectra, i.e., that have a frequency-independent spectral density at low frequency and drop off much faster than $1/f$ at high frequencies (see spectrum 1 in Fig. 4). In contrast, noise measured at fields where $\eta_{12}^2 \approx 0.01$ showed $1/f$-like spectra (e.g., see spectrum 2 in Fig. 4). Large coherence values and Lorentzian spectra were also observed near 29 and 49 mT, where the *pinned* layer is undergoing reversal. These Lorentzian spectra are attributed to a macroscopic magnetization process and suggest that domain wall propagation, or domain wall hopping between two or among more pinning sites, introduces large spatial correlation in the measured low-frequency noise spectra. This behavior differs from the absence of coherence for MR $1/f$ noise, which is due to the superposition of a large number of independent magnetic fluctuators, each of which has a similar magnitude. The increase in coherence in Fig. 8, presence of Lorentzian-like spectra, and deviations from an inverse volume scaling of the magnetic noise are indicative of the noise being principally due to a small number of large magnetic fluctuators.

Comparing Figs. 8 to 7 highlights the importance of domain structure engineering for attaining well-defined crossed-anisotropy geometry in magnetic sensor designs. In devices where the magnetization reversal process is poorly defined, macroscopic fluctuations create undesired excess noise at low frequencies. Large two-level fluctuators, with a $1/f^2$ noise spectrum, can be effectively suppressed when the magnetization reversal process proceeds smoothly by coherent rotation, just as in the ideal case of a Stoner-Wohlfarth particle when the external field is applied transverse to its easy-axis.[27]

An upper limit for the fluctuating magnetic volume can be set by considering that $1/f$ spectra (not shown) were also observed in other $w = 0.6\,\mu$m (type C) yoke samples that have a lateral spacing between electrodes as small as 300 nm. As a rule of thumb,[3] a featureless $1/f$ noise spectrum results from a

superposition of more than one active two-level fluctuator per octave of frequency. In our 1-kHz measurement bandwidth, there must exist at least 10 fluctuators in this subvolume to give the featureless $1/f$ spectrum, suggesting upper limits of $9 \times 10^4$ and $4.5 \times 10^4$ $nm^3$ for the fluctuating magnetic volume of the free and pinned layers, respectively. This is roughly 10 times smaller than the limit reported by Petta *et al.*,[28] in SV bridge sensors. Since the exchange length is comparable to the film thickness, we take the thickness of the magnetic fluctuator to be that of the magnetic film. The in-plane separation of the magnetic fluctuators in our sensor is therefore ~135 nm.

## IV. DISCUSSION

The preceding results raise the following question: What are the elementary magnetic fluctuators? Micromagnetic simulations of yoke-shaped sensors indicate that the long arm of the yoke is in a single domain state.[29] This suggests long-range spatial correlations of the noise, which are not observed (except in the collinear configuration, which is not a sensor). At the opposite extreme, a magnetic volume on the scale of the exchange length $4^3$ $nm^3$[30] is expected to behave as a single domain particle and give rise to white noise at low frequency and a noise peak at the ferromagnetic resonance frequency.[19] The nanopolycrystalline nature of sputtered SV films often leads to magnetization dispersion, i.e., so-called magnetization ripple, which manifests itself as quasiperiodic variations perpendicular to the mean magnetization direction.[31] The ripple wavelength is known to depend on the magnetic anisotropy field $H_K$, and at remanence, Hoffman theory[32] predicts it is proportional to $(H_K)^{-1/2}$. In soft magnetic thin films, such as permalloy, the ripple wavelength tends to be several hundred nanometers.[33] Coherent magnetization fluctuations over these length scales would lead, in our smallest devices, to spatial correlations in the noise, which were not detected.

Another candidate is magnetic inhomogeneities on the scale of the grain size. In sputtered soft magnetic films, this size is typically between 10 and 120 nm.[34] Grain boundaries weaken the exchange interaction between spins, while within a grain strong exchange coupling leads to uniform magnetization. In a single domain state, the magnetization vector in an isolated grain can fluctuate within a small angle around its equilibrium value. The equilibrium angle is determined by the minimum in the magnetic energy density of the grain. For example, in the Stoner-Wohlfarth model[27] for an isolated magnetic particle that has uniaxial anisotropy, the energy density has a double well profile as a function of the magnetization's angle with respect to the anisotropy direction. In a film, competition between underlying disorder (e.g., random anisotropy) and interactions (e.g., exchange and magnetostatic) between grains gives rise to nontrivial energy landscapes. It is conceivable that for any grain there exist magnetic configurations of nearly equivalent energy separated by an energy barrier. Thermally driven transitions between two magnetic states separated by a barrier a few times the available thermal energy would give rise to low-frequency fluctuations. In a SV, magnetization fluctuations and sample resistance are coupled by the GMR effect, so a superposition of a large number of grains that have two-state magnetization fluctuations with a suitably broad distribution of time scales gives the observed $1/f$ noise.[3] The existence of an ensemble of small magnetic fluctuators is supported by Lorentz microscopy images that show localized magnetic fluctuators flip-flopping between two configurations (e.g., see Fig. 2 in Ref. 20).

At present, a clear understanding of the precise microscopic nature of MR $1/f$ noise is lacking. For instance, it was shown previously that a "macrospin" model can predict the form of excess noise as a function of magnetic field in micrometer-size SV devices.[35,36] In this approach, the free ferromagnetic layer is treated as a macrospin, whose magnetization direction is perturbed by thermal fluctuations. Hill and Nor[35] suggested that the effective volume for the macrospin is ~$10^{10}$ $nm^3$. The noise volume scaling and strongly localized magnetic fluctuators observed in our present work are obviously not captured by this model. Also, it is not evident how a broad band $1/f$ spectrum emerges from such macrospin models. An alternative model for magnetic $1/f$ noise is based on dynamical heterogeneity involving localized magnon relaxation.[37] A key feature of this model is that relaxation rates vary exponentially with inverse size of the so-called correlated regions, which can be on the order of the magnetic exchange length. Such a short length scale is consistent with the absence of spatial correlations in the measured noise. Also, the inverse size scaling leads to asymmetrical deviations from $1/f$ behavior. However, our experimental bandwidth was too narrow to draw conclusions about asymmetries in the shape of the noise spectra. Finally, although this model accurately describes the observed slow magnetic relaxation in, e.g., iron whiskers,[38] the extent of its applicability to our devices in which the internal fields are much larger than zero is not clear.

## V. CONCLUSION

We used resistance noise to study slow kinetics (>1 ms) of the micromagnetic structure in yoke-shaped GMR SVs with crossed anisotropy. The yoke-shaped geometry promotes uniform magnetization along the long arm of the yoke and leads to a linear, low hysteretic response of the free (soft) magnetic layer, which is desirable for sensor applications. The resistance noise near the magnetic transition regions is due to quasiequilibrium magnetization fluctuations that couple to the resistance through the GMR effect. Noise spectra are $1/f$-like, and the absence of spatial correlations in the noise power between adjacent voltage taps along the arm of the yoke puts an upper bound of 135 nm for the lateral length scale of the magnetic fluctuators. The noise power also scales inversely with the distance between voltage taps. These results indicate that an ensemble of magnetic fluctuators exists, possibly due to disorder on the scale of the microstructural grain size in the sputter-deposited magnetic films.

The dissipative processes that lead to the MR $1/f$ noise occur at the nanoscale and can be attributed to reversible magnetic reconfigurations that occur through thermal activation over a barrier. At present, the microscopic mechanisms that govern MR noise are not fully understood. Further experimental and theoretical investigations are required to provide guidance in the search for low-noise magnetic materials and device designs to support improvements in the low-frequency signal-to-noise ratios of GMR and TMR sensors. Finally, any

*khaughey@udel.edu

[1] H. Barkhausen, Physik Z **20**, 401 (1919).

[2] Sh. Kogan, *Electronic Noise and Fluctuations in Solids* (Cambridge University Press, Cambridge, 1996).

[3] M. B. Weissman, Rev. Mod. Phys. **60**, 537 (1988).

[4] R. de Sousa, Phys. Rev. B **76**, 245306 (2007).

[5] S. Vitale, G. Cerdino, A. Prodi, A. Cavalleri, P. Falferi, and A. Maraner, in *Quantum Tunneling of Magnetization—QTM '94*, edited by L. Gunther and B. Barbara (Kluwer, Norwell, MA, 1995), pp. 157.

[6] L. Faoro and L. B. Ioffe, Phys. Rev. Lett. **100**, 227005 (2008); S. Sendelbach, D. Hover, A. Kittel, M. Mück, J. M. Martinis, and R. McDermott, *ibid*. **100**, 227006 (2008).

[7] S. A. Wolf, D. D. Awschalom, R. A. Buhrman, J. M. Daughton, S. von Molnar, M. L. Roukes, A. Y. Chtchelkanova, and D. M. Treger, Science **294**, 1488 (2001).

[8] J. Foros, A. Brataas, G. E. W. Bauer, and Y. Tserkovnyak, Phys. Rev. B **79**, 214407 (2009).

[9] S. Kang, JOM **60**, 28 (2008).

[10] W. F. Egelhoff Jr., P. W. T. Pong, J. Unguris, R. D. McMichael, E. R. Nowak, A. S. Edelstein, J. E. Burnette, and G. A. Fischer, Sensor. Actuator. Phys. **155**, 217 (2009).

[11] R. McDermott, IEEE Trans. Appl. Supercond. **19**, 2 (2009).

[12] H. T. Hardner, M. B. Weissman, M. B. Salamon, and S. S. P. Parkin, Phys. Rev. B **48**, 16156 (1993).

[13] E. R. Nowak, M. B. Weissman, and S. S. P. Parkin, Appl. Phys. Lett. **74**, 600 (1999).

[14] F. N. Hooge, Physica (Utrecht) **60**, 130 (1972).

[15] L. Jiang, E. R. Nowak, P. E. Scott, J. Johnson, J. M. Slaughter, J. J. Sun, and R. W. Dave, Phys. Rev. B **69**, 054407 (2004).

[16] A. Ozbay, A. Gokce, T. Flanagan, R. A. Stearrett, E. R. Nowak, and C. Nordman, Appl. Phys. Lett. **94**, 202506 (2009).

[17] N. Smith, A. M. Zeltser, D. L. Yang, and P. V. Koeppe, IEEE Trans. Magn. **33**, 3385 (1997).

[18] R. Stearrett, W. G. Wang, L. R. Shah, J. Q. Xiao, and E. R. Nowak, Appl. Phys. Lett. **97**, 243502 (2010).

[19] N. Smith and P. Arnett, Appl. Phys. Lett. **78**, 1448 (2001).

[20] J. M. Shaw, R. Geiss, and S. Russek, Appl. Phys. Lett. **89**, 212503 (2006).

[21] B. Raquet, M. Viret, M. Costes, M. Baibich, M. Pannetier, M. Blanco-Mantecon, H. Rakoto, A. Maignan, S. Lambert, and C. Fermon, J. Magn. Magn. Mater. **258-259**, 119 (2003).

[22] Y. Wei, R. E. Jones, and M. H. Kryder, J. Appl. Phys. **81**, 4918 (1997).

[23] M. Pannetier, C. Fermon, G. Le Goff, J. Simola, and E. Kerr, Science **304**, 1648 (2004).

[24] F. Guo, G. McKusky, and E. D. Dahlberg, Appl. Phys. Lett. **95**, 062512 (2009).

[25] C. Ren, X. Liu, B. D. Schrag, and G. Xiao, Phys. Rev. B **69**, 104405 (2004).

[26] J. H. Scofield, D. H. Darling, and W. W. Webb, Phys. Rev. B **24**, 7450 (1981).

[27] E. C. Stoner and E. P. Wohlfarth, Phil. Trans. Roy. Soc. Lond. Math. Phys. Sci. **240**, 599 (1948).

[28] J. R. Petta, T. Ladd, and M. B. Weissman, IEEE Trans. Magn. **36**(4), 2057 (2000).

[29] C. Fermon, M. Pannetier-Lecoeur, N. Biziere, and B. Cousin, Sensor. Actuator. Phys. **129**, 203 (2006).

[30] J. M. D. Coey, *Magnetism and Magnetic Materials* (Cambridge University Press, New York, 2010).

[31] C. K. Lim, J. N. Chapman, M. Rahman, A. B. Johnston, and D. O. O'Donnell, J. Appl. Phys. **95**, 1510 (2004).

[32] H. Hoffmann, IEEE Trans. Magn. **4**, 32 (1968).

[33] A. Gentils, J. N. Chapman, G. Xiong, and R. P. Cowburn, J. Appl. Phys. **98**, 053905 (2005).

[34] J. W. Freeland, K. Bussmann, and Y. U. Idzerda, Appl. Phys. Lett. **76**, 2603 (2000); Y. C. Wang, J. Ding, J. B. Yi, B. H. Liu, T. Yu, and Z. X. Shen, **282**, 211 (2004).

[35] E. W. Hill and A. F. Nor, IEEE Trans. Magn. **37**, 2031 (2001).

[36] R. J. M. van de Veerdonk, P. J. L. Belien, K. M. Schep, J. C. S. Kools, M. C. de Nooijer, M. A. M. Gijs, R. Coehoorn, and W. J. M. de Jonge, J. Appl. Phys. **82**, 6152 (1997).

[37] R. V. Chamberlin, J. Appl. Phys. **76**, 6401 (1994).

[38] R. V. Chamberlin and M. R. Scheinfein, Science **260**, 1098 (1993).